Analyst

Differential Detection of Immune Cell Activation by Label-free Radiation Pressure Force

Journal:	*Analyst*
Manuscript ID	AN-ART-06-2021-001066.R1
Article Type:	Paper
Date Submitted by the Author:	08-Jul-2021
Complete List of Authors:	Lu, Qin; US Naval Research Laboratory, Chemistry Division Barlow, Daniel; US Naval Research Laboratory, Chemistry Division Haridas, Dhanya; US Naval Research Laboratory, Chemistry Division

Differential Detection of Immune Cell Activation by Label-free Radiation Pressure Force

Qin. Lu, Daniel. E. Barlow, Dhanya Haridas*

Naval Research Laboratory, Chemistry Division, 4555 Overlook Ave., S.W. Washington, D.C. 20375

*Corresponding Author
E-mail: qin.lu@nrl.navy.mil.

ABSTRACT

Label-free radiation pressure force analysis using a microfluidic platform is applied to the differential detection of innate immune cell activation. Murine-derived peritoneal macrophages (IC-21) are used as a model system and the activation of IC-21 cells by lipopolysaccharide (LPS) and interferon gamma (IFN-γ) to M1 pro-inflammatory phenotype is confirmed by RNA gene sequencing and nitric oxide production. The mean cell size determined by radiation pressure force analysis increases slightly after the activation (4 to 6 %) and the calculated percentage of population overlaps between the control and the activated group after 14 and 24 h stimulations are at 79% and 77 %. Meanwhile the mean cell velocity decreases more significantly after the activation (14% to 15%) and the calculated percentage of population overlaps between the control and the activated group after 14 and 24 h stimulations are only at 14 % and 13 %. The results demonstrate that the majority of the activated cells acquire a lower velocity than the cells from the control group without changes in cell size. For comparison label-free flow cytometry analysis of living IC-21 cells under the same stimulation conditions are performed and the results show population shifts towards larger values in both forward scatter and side scatter, but the calculated percentage of population overlaps in all case are significant (70% to 83 %). Cell images obtained during radiation pressure force analysis by a CCD camera, and by optical microscopy and atomic force microscopy (AFM) reveal correlations between the cell activation by LPS/IFN-γ, the increase in cell complexity and surface roughness, and enhanced back scattered light by the activated cells. The unique relationship predicted by Mie's theory between the radiation pressure force exerted on the cell and the angular distribution of the scattered light by the cell which is influenced by its size, complexity, and surface conditions, endows the cell velocity based

measurement by radiation pressure force analysis with high sensitivity in differentiating immune cell activation.

Keywords Radiation Pressure Force, Innate immune cells, Macrophages, Label-free, Living cells, Scattered light

INTRODUCTION

The innate immune system is composed of first responder cells including neutrophils, macrophages, dendritic cells, and natural killer cells. The response of innate immune cells to pathogen are typically rapid and can be triggered without the selective events that underlie adaptive immunity, which is characterized by antigen-specificity and immunological memory.[1] Hence innate immune cells may be able to serve as living sensors for early stage detection of pathogen infection. Macrophages, distributed widely in organs and connective tissue, play central roles in innate as well as adaptive immunity. Macrophages operate in host defense through phagocytosis, secreting cytokines to initiate pro-inflammatory reaction against the invading microbes, presenting antigen to activate the T lymphocytes in adaptive immunity, and promote the repair of damaged tissues and the restoration to homeostasis.[2] Macrophages have remarkable plasticity and take a variety of phenotypes based on the stimuli and their functions.[3] They can be classically activated (M1 pro-inflammatory phenotype) in the presence of microbial products such as lipopolysaccharide (LPS), with interferon gamma (IFN-γ) produced by innate immune cells such as natural killer (NK) cells and by adaptive immune cells such as T helper 1 cells and CD8+ cytotoxic T cells.[4, 5] During an inflammatory response to pathogenic stimulation, macrophages undergo striking changes in their morphology as well as metabolism.[6,7,8]

Conventional approaches to detect the activation of macrophages by infectious agents involve identification and quantification of cell surface markers, cytokines, and transcription factors, based on prior knowledge on the infectious agents. These approaches normally are limited to the known targets and require cell labeling. Furthermore the process of labeling the cell with biomarkers may alter the physiological states of the cells. Label-free detection and characterization methods overcome these obstacles and allow for living cell analysis by detecting the changes in cell intrinsic properties such as morphology, refractive index, compressibility, and deformability upon exposure to infectious agents. Label-free living immune cell detection holds the potential to rapidly detect an early onset infection manifested by a cell population shift based on these intrinsic properties without relying on specific antibodies or targeting specific molecules. If a population shift has been confirmed, more specific analyses can be initiated to reach a correct diagnosis.

Progresses and innovations in microfluidic technologies have accelerated the development of label-free microfluidic techniques towards single-cell analysis and sorting. Carey et al. classified these techniques under four broad areas: 1) electrical, 2) optical, 3) hydrodynamic, and 4) acoustic.[9] Label-free optical cell analysis can be divided into two classes. Optical tweezers, invented by Ashkin,[10] traps and manipulates living cells using a tightly focused laser beam,[11] stretches the cell and measure its deformability[12] or rotates the cell and allows for tomographic reconstruction of the 3D structure of the cell through continuous imaging[13] using two divergent laser beams. Optical chromatography, invented by Imasaka et al.,[14] utilizes two opposing forces: radiation pressure force from a loosely focused laser beam and viscous drag force from a fluid flow in a microfluidic channel. It has been used in the measurements of erythrocyte elasticity by deform cells using a shear stress generated by the fluid flow,[15] and to monitor vesicular

stomatitis virus infection in Vero (African green monkey kidney) cells by size normalized velocity.[16] Recently, a microfluidic based label-free high-speed imaging method was applied to the drug susceptibility testing of leukemia with extreme-throughput (>1 million cells per s) and enabled image-based identification of the drug susceptibility of every single white blood cell in whole blood within 24 hours.[17]

In this study, applying the principle of optical chromatography on a microfluidic device, the immune response of murine-derived peritoneal macrophages (IC-21) to inflammatory stimulation and their activation to M1 pro-inflammatory phenotype is sensitively detected. The activation of IC-21 cells to M1 type cells induces negligible changes in cell size and refractive index but marked increases in cell complexity and surface roughness. Cell velocity, a key parameter obtained from label free radiation pressure force analysis, directly correlates to the magnitude of the radiation pressure force which is influenced by cell size, refractive index, complexity and surface roughness. Collectively M1 type IC-21 cells form a distinctly "slower" population separated from the cells of the control group. The data collected during the analysis also includes the image of each cell which provides information about the cell size and morphology. The population shift upon activation detected by label-free radiation pressure force analysis based on the cell velocity is compared with that detected by the standard label-free flow cytometry based on forward and side scatter. Because of the strong dependence of radiation pressure force on the angular distribution of the scattered light by the cells predicted by Mie theory,[18] radiation pressure force analysis demonstrates much higher sensitivity to changes in cell complexity and surface condition.

MATERIALS AND METHODS

Cell culture and stimulation

Murine-derived peritoneal macrophages (IC-21) were obtained from ATCC (Manassas, VA, USA). Cells were cultured in RPMI-1640 medium supplemented with 10% fetal calf serum (ATCC) and maintained in a 5% CO_2, 37°C humidified incubator. Stimulated cells were cultured in 6-well plates (USA Scientific, Ocala, FL) in the presence of 1μg/ml LPS from *Escherichia coli* (Sigma-Aldrich, St. Louis, MO) and 50 U/ml murine recombinant (IFN-γ (Sigma-Aldrich) for a period of 14 and 24 h. Control cells were cultured in a similar manner in the absence of LPS and IFN-γ.

RNA isolation and sequencing

Cells cultured in 6-well plates were first washed twice with PBS (1X, Life Technologies, Carlsbad, CA) and then were dislodged from the well surface by incubating with 2 mL PBS for 7 min at 37°C. Dislodged cells were transferred to centrifuge tubes and centrifuged at 150 × *g* for 5 min. The cell pellets were collected and RNA extraction was performed with the miRNeasy Mini Kit (Qiagen, Germantown, MD), according to the manufacturer's protocol. Quality and quantity of RNA were initially determined by the value of absorbance ratio A_{260nm}/A_{280nm} using a NanoDrop 2000 Spectrophotometer (Thermo Fisher Scientific, Waltham, MA). All six samples (3 × control and 3 × LPS/IFN-γ 24 h stimulation) have an A_{260nm}/A_{280nm} ratio ≥ 2.05. The qualities of the samples were further assessed using Agilent Tapestation (Agilent Technologies, Palo Alto, CA) for RNA integrity number (≥ 9.7). The RNA-Seq analysis (n = 3/group) was performed by GENEWIZ (South Plainfield, NJ).

Griess assay for nitric oxide production

The assay was performed using Promega Griess Reagent System (Promega Corporation Madison, WI) on a SPECTRONIC™ 200 Spectrophotometer (Thermo Scientific™).

Cell culture supernatants from IC-21 cells before and after stimulated with LPS/IFN-γ for 14 and 24 h were collected in centrifuge tubes (n = 3/group) and centrifuged at 300 × g for 5 min to remove any debris. In a 1-cm path length cuvette 300 µl clear supernatant was first mixed with 300 µl sulfanilamide solution and incubated in the dark at room temperature for 10 min. 300 µl *N*-1-napthylethylenediamine dihydrochloride (NED) solution was added to this mixture and incubated another 10 min in the dark before the absorbance of the final mixture at 545 nm was recorded by the spectrophotometer. The concentration of nitric oxide was determined from a calibration curve created from sodium nitrite concentrations ranging from 0 - 100 µM prepared in the same culture medium (RPMI 1640 containing 10% serum). Cell counts (~ 6 x 10^5 cells) were obtained using a hemocytometer by counting the dislodged cells after the cell culture supernatant was removed.

Cell preparation for radiation pressure force and flow cytometry analyses

Adherent cells (control and stimulated) were first washed twice with PBS and then were dislodged from the well surface by incubating with 2 mL PBS at 37°C for 7 min. The cells were transferred to centrifuge tubes and centrifuged at 150 × g for 5 min. After discarding the supernatant, the cell pellet was re-suspended in PBS and transferred to a 2 mL screw cap tube. A cell density of 2 × 10^5 cells/ml was used for radiation pressure force analysis and a cell density of 1 × 10^6 cells/ml was used for flow cytometry.

Microfluidic system of cell analysis using radiation pressure force

Microfluidic system comprises the following components. (1) A microfluidic flow cell is constructed with a serpentine channel to disperse cells enabling single-file cell injection, a 3D focusing nozzle connecting to the serpentine channel and three sheath flow channels to focus the cells at the center of a focusing channel, and a detection channel in which cells encounter the laser

beam (Figure 1). (2) A pneumatic flow system consists of five electronic pressure controllers (OEM-EP, Parker Hannifin, Hollis, NH) to pressurize fluid reservoirs connected to the three sheath flow channels, the serpentine injection channel, and the outlet channel of the flow cell, enabling the pulseless and reproducible fluid flow. 3) An optical system includes a continuous wave (CW) 1064 nm ytterbium fiber laser (IPG Photonics, Oxford, MA) and a 75 mm focal length lens to provide a mildly focused laser beam. (4) An imaging system consists of a 10 × objective (Mitutoyo, Kawasaki, Japan) and a lens tube system (Infinity Photo Optical, Boulder, CO) connected to a CCD camera (piA 1600-35 gc, Basler, Inc. Exton, PA), facilitating the alignment of the laser beam into the detection channel and the observation of cell movement. (5) A data collection and analysis system includes a CCD camera and in-house software developed using LabView. Cells carried by the fluid travel through the detection channel in single file and their movements were decelerated by an incident laser beam propagating in the opposite direction of the fluid flow. Cell velocities were calculated from the captured cell images and their positions relative to the flow path of the detection channel. The average particle size was determined by counting the number of pixels in the images captured by a CCD camera using an OD = 3.0 NIR absorptive ND filter (Thorlabs Inc. Newton, New Jersey). Images of cells with observable scattered laser light were captured using an OD = 2.0 NIR absorptive ND filter. The throughput of the analysis was ~ 500 cells/min.

Flow cytometry

The control and stimulated cells were suspended in 1 ml ice-cold PBS. Each sample was analyzed by a BD Accuri C6 plus flow cytometer (BD Biosciences, San Diego, CA, USA) with a limit of 100000 events. The forward scatter (FSC) and side scatter (SSC) data were analyzed using BD Accuri C6 plus software (version 1.0.23.1) and Origin 2015.

Cell fixation and staining

Fixed suspension cells were prepared as described below. The adherent cells (control and stimulated) were first washed twice with PBS and then were dislodged from the well surface by incubating with 2 mL PBS at 37°C for 7 min. Cells were transferred to the centrifuge tubes and centrifuged at 150 x *g* for 5 min. After discarding the supernatant, the cell pellet was re-suspended in PBS. An equal volume of 4% paraformaldehyde (Sigma-Aldrich, St. Louis, MO) was added to the cell suspension and the resulting mixture was incubated for 10 min at room temperature before the mixture was centrifuged at 150 x *g* for 5 min. The supernatant was discarded and the fixed cell pellet was re-suspended in 2 ml PBS. The cell suspension was transferred to a poly-D-lysine coated FluoroDish cell culture dish (World Precision Instruments, Sarasota, FL) and cells were ready to be imaged after they settled at the bottom of the cell culture dish. Fixed and stained adherent cells were prepared as described below. The adherent cells (control and stimulated) were washed twice with PBS and fixed with 3.7% methanol-free formaldehyde solution (Sigma-Aldrich, St. Louis, MO) in PBS for 15 min at room temperature. Fixed cells were then washed twice with PBS and permeabilized in 0.1% Triton™ X-100 (Sigma-Aldrich, St. Louis, MO) in PBS for 15 min. To reduce nonspecific background staining 1% BSA (ThermoFisher Scientific, Pittsburgh, PA) was added to the sample followed by 30 min incubation at room temperature. After washing the sample twice with PBS, 300 µl Alexa Fluor 488 phalloidin (495/518 nm, ThermoFisher Scientific) solution diluted in PBS, for the selective staining of F-actin, was added and the sample was incubated in the dark for 30 min at room temperature. The cells were washed twice with PBS and 300 µl DAPI nucleic acid stain (Ex/Em: 358/461 nm, ThermoFisher Scientific) solution diluted in PBS was added on the cells. After 5 min the sample was washed twice with PBS and was ready for imaging.

DIC and confocal fluorescence microscopy

DIC images of fixed suspended cells were acquired on a Nikon Eclipse Ti inverted confocal microscope (Nikon Instruments Inc. Melville, NY) with a 100x oil-immersion objective lens (NA 1.49, Nikon). DIC images and confocal fluorescence images of fixed and stained adherent cells were acquired on the same microscope equipped with a 405 nm OBIS laser and a 488 nm Sapphire laser (both from Coherent, Santa Clara, CA).

Atomic Force Microscopy analyses of living IC-21 cells

Cells (control and stimulated) were scanned using a NanoWizard 4a AFM (Bruker Nano GmbH**,** Berlin, Germany**)** mounted on an Eclipse Ti-*E* Inverted Microscopes (Nikon Instruments Inc. Melville, NY). Cell images were obtained in QI mode at 37 °C using qp-BioAC-CB3 AFM probes (NANOSENSORS, CH-2000 Neuchatel, Switzerland) with a set point of 400 pN.

Statistical analysis

Each experiment was repeated at least three times. For differential gene expression analysis, the Wald test was used to generate *p*-values and $\log_2$ fold changes. Genes with an adjusted *p*-value < 0.05 and absolute $\log_2$ fold change > 1 were called as differentially expressed genes. For data collected from radiation pressure force and flow cytometry, comparisons between the control groups and the activated groups were made by two-sample t-test. A *p*-value < 0.05 was considered to be statistically significant.

RESULTS AND DISCUSSIONS

Confirming M1 pro-inflammation phenotype by RNA gene sequencing analysis and nitric oxide production

IC-21 macrophage cell line is derived from SV40 transformed mouse peritoneal macrophages. It shares many properties with normal mouse macrophages including phagocytosis,[19] cytokine

production,[20, 21] and activation by LPS via toll-like receptor 4 (TLR4). When macrophages are classically activated by LPS/IFN-γ into M1 pro-inflammatory phenotype, they secrete pro-inflammatory cytokines, such as tumor necrosis factor (TNFα), IL-1β, IL-6, and IL-12β. RNA sequencing analysis of IC-21 cells before and after 24 h LPS/IFN-γ stimulation reveals that the genes encoding for TNFα, IL-1β, IL-6, and IL-12β in the stimulated group are significantly upregulated (Figure 2a). In response to the stimulation of LPS/IFN-γ and the production of the pro-inflammation cytokines, the expression of inducible nitric oxide synthase (iNOS)[22] in the stimulated group is also highly induced (Figure 2a). As a result of iNOS expressional induction, nitric oxide was produced continuously and its concentrations were measured by the Griess assay at 14 and 24 h LPS/IFN-γ stimulation (Figure 2d). It is noted that the production of nitric oxide is one of the most reliable ways to confirm the M1 pro-inflammatory phenotype in murine macrophages.[23]

In addition to the upregulation of genes encoding the well-known pro-inflammatory cytokines, three newly identified novel distinct M1 genes, CD38, G-protein coupled receptor 18 (Gpr18), and formyl peptide receptor 2 (Fpr2),[24] were also found to be upregulated in IC-21 after LPS/IFN-γ stimulation (Figure 2b). Under the condition and the concentrations of LPS and IFN-γ used in this work, IC-21 macrophages were indeed classically activated into M1 phenotype.

Furthermore, response gene to complement 32 (RGC-32), an important regulator in phagocytosis and F-actin formation/assembling,[25] and vasodilator-stimulated phosphoprotein (VASP) involved in the assembly of actin filament networks,[26] were also upregulated (Figure 2c). The upregulation of these two genes implicate that stimulated IC-21 cells undergo the actin cytoskeleton modification.

Label-free living cell analysis using radiation pressure force and flow cytometry

The results from radiation pressure force analysis of living IC-21 cells before and after 14 and 24 h LPS/IFN-γ stimulation are given in Figure 3 and Figure 4. Figure 3a and 3b present the histograms of the distribution of cell diameters within each group and between the groups. A small but statistically significant ($p < 0.001$) population shift to larger cell diameters after LPS/IFN-γ stimulation is detected. In the 14 h stimulation experiment, the mean cell diameter value for the control group (582 cells) is 10.44 ± 1.19 μm. An increase of ~ 4 % (10.87 ± 1.20 μm) is measured for the activated group (604 cells). In the 24 h stimulation experiment, the mean cell diameter value for the control group (511 cells) is 10.14 ± 0.82 μm, and an increase of ~ 6 % (10.77 ± 0.73 μm) is measured for the activated group (513 cells). Figure 3c and 3d present the histograms of the distribution of cell velocity within each group and between the groups. In the 14 h stimulation experiment, the mean cell velocity for the control group (582 cells) is 625.95 ± 26.02 μm/s, a decrease of 14 % to 538.91 ± 32.37 μm/s for the activated group (604 cells) is detected. In the 24 h stimulation experiment, the mean cell velocity for the control group (511 cells) is 653.58 ± 49.59 μm/s, and a decrease of 15 % to 553.28 ± 30.07 μm/s for the activated group (513 cells) is detected. The separation between the activated group and the control group based on cell size and cell velocity can be assessed by the calculated percentage of population overlap. In terms of the cell diameter significant population overlaps, > 77 %, are present at 14 and 24 h stimulations, suggesting a minor population shift to larger cell size upon LPS/IFN-γ stimulation. On the contrary the population shifts based on cell velocity at both 14 and 24 h are much more prominent. The calculated percentage of population overlap between the control and the activated groups are only at 13 % and 14% for 14 h and 24 h stimulation, respectively, with the cells from the activated group displaying lower velocities. The plots of cell diameters vs. cell velocities are given in Figure 3e and 3f. Evidently the majority of cells from the activated group shift away from the control

group to a lower cell velocity even though their cell diameters fall within the same range of the control group, suggesting that other characters of the cells, other than the cell size, must have changed and are sensitively detected by the measurement in cell velocity. Figure 4a shows cell images captured by a CCD camera during the analysis when the cell is traveling through the detection channel using an OD = 3.0 NIR absorptive ND filter for attenuating the laser light at 1064 nm. These images together with their recorded positions relative to the flow path of the detection channel are used to calculate the cell velocities and sizes. The cells from both the control and the activated groups are nearly spherical-shaped, but the "contour" of the cells from the activated group are much rugged. Cell images in Figure 4b are captured with an OD = 2.0 NIR absorptive ND filter to allow observation of the scattered laser light. Cells from the activated group display increased laser light scatter, especially in the direction opposite to the laser beam (backward scatter).

For comparison, label-free flow cytometry analysis of living IC-21 cells are performed. The results are presented in Figure 5 as the histograms of the distribution of FSC-A (Forward Scatter Area) and SSC-A (Side Scatter Area) within each group and between the groups. Both FSC-A and SSC-A recorded for 14 h and 24 h stimulations show small but statistically significant ($p < 0.001$) population shift towards larger FSC-A and SSC-A values after LPS/IFN-γ stimulation. The intensity of FSC-A, detected along the direction of propagation of the incident laser beam, reflects the size of the cells. Thus the shifts in Figure 5a and 5b again show a minor increase in cell size in the activated groups, in agreement with the results from radiation pressure force analysis (Figure 3a and 3b). The intensity of SSC-A, recorded at 90 ° of the incident laser beam, is affected by multiple biophysical characteristics of the cells, i.e., the presence of granules and vesicles or vacuoles in cytoplasm, the roughness of the cell membrane, as well as the cell size. Any internal

and surface irregularities, including cytoplasmic granules, vesicles, and other organelles and membrane roughness will typically contribute to SSC signals.[27] The shifts in Figure 5 c and 5 d to larger SSC-A values suggest an increase in cell complexity together with a small increase in cell size revealed by the increased in FSC-A values, in the stimulated groups. In all cases the calculated percentage of population overlap is significant (≥ 70%).

Characterization of cell morphology by optical microscope and atomic force microscope

The examination of the cell morphology that closely resembles the living cells analyzed by the radiation pressure force and flow cytometry is enabled by DIC images of fixed suspension cells. Cells from the control group (Figure 6a) are spherical in shape and have relatively smooth and well-defined cell boundary. Cells from the activated group (Figure 6b) are similar in size and shape to those of the control group, but a roughness of the cell boundary and the complexity in cell structure is notably increased.

DIC images and confocal fluorescence images of fixed and stained adherent cells from the control and the activated groups are shown in Figure 7. Distinctive differences between the two groups are revealed by DIC images and confocal fluorescence images of cells stained for their F-actin filaments and nuclei using Alexa Fluor 488 phalloidin and DAPI, respectively. The most prominent feature in DIC images is the appearance of multiple vacuole-like structures in the activated group (Figure 7b). The formation of vacuoles in LPS-stimulated macrophage cells are also observed in RAW 264.7 cells,[28] J774.1 cell line,[29] and JY3 cell line,[30] even though there is no consensus on the origin of vacuoles. In confocal fluorescence images, the difference between the control group and the activated group is the extent of formation and the distribution of F-actin rich dot-like structures. In the control group (Figure 8a), these dot-like structures mainly localized near the periphery of the cell lamella. In the activated group (Figure 8b) these structures form more

extensively and spread widely over the cell. AFM images acquired on living cells also reveal marked differences in surface morphology between the control group and the activated group. AFM images, especially the deflection images, show that the surface of the control cells is smooth (Figure 8a) and the surface of the activated cells (Figure 8b) is "studded" with numerous dot-like and short rod-like structures. Pi et al.[31] also observed that upon stimulating RAW 264.7 macrophages with LPS, the size of the surface particle structures and the roughness of membrane significantly increased. They attributed these observations to the clustering of membrane proteins. The results from optical microscopy and atomic force microscopy indicate that there are marked differences in cell morphology and cell surface condition between the activated group and the control group. These results are the manifestation of the upregulated genes RGC-32 and VASP (Figure 2c) and demonstrate that F-actin formation/assembling and the cytoskeleton reorganization are involved in the activation of IC-21 cells by LPS/IFN-γ stimulation.

Discussions

To understand why cell velocity based measurement by radiation force analysis provides a more sensitive detection for differentiating immune cell activation than label-free flow cytometry (FSC-A an SSC-A), a close examination at the radiation pressure force is necessary. Governed by the law of conservation of momentum, the radiation pressure force exerted on a particle is the result of a momentum transfer from the laser light to the particle. It is proportional to the amount of forward momentum that is removed from the incident light by the particle through scatter or absorption and is not replaced by the forward component of the momentum carried by the scatted light.[18] The radiation pressure force from a Gaussian beam exerted on a non-absorbing spherical particle with real refractive index (RI) is given by[32,33]

$$F_{pr} = \frac{2Pn_1}{c}\left(\frac{a}{\omega 0}\right)^2 \times Q_{ext}(1 - < cos\theta >) \qquad [1]$$

where P denotes the laser power, c is the phase velocity of the light, n_1 is the RI of surrounding medium, a is the radius of the spherical particle and ω_0 is the beam radius determined experimentally.[34] Q_{ext} is the extinction efficiency factor and a function of the particle size and RI and its value increases when the particle size or RI is increased. $<cos\theta>$, termed as the asymmetry factor in which θ is the scattering angle formed by the incident light and the scattered light, is the mean over the sphere of the cosine of the scattering angle, weighted by the phase function.[18] The value of asymmetry factor reflects the relative importance of forward-to-backward scatter by the particle and decreases when the ratio of forward-to-backward scatter is decreased. The exact solution of Equation [1] is limited to the special cases of simple spherical particles. In the analysis using radiation pressure force, laser power P, the RI of surrounding medium n_1, and the beam radius ω_0 were kept constant (3 W, 1.326, and 19.8 μm). The impact on F_{pr} from the cell itself includes its size, RI, and the angular distribution of the scattered light by the cell which depends greatly on its composition and the surface condition.

When IC-21 cells were stimulated by LPS/IFN-γ, the majority of the cells displayed little to no change in their size, as determined by the cell size measurement using radiation pressure force analysis and supported by the results from flow cytometry (FSC-A). In our previous work on *Bacillus anthracis* spore uptake by macrophage cells, the bulk RI of a macrophage (RI: 1.384) engulfed 22 spores (RI: 1.528) was calculated using the Maxwell Garnett Approximation,[35] and the RI value obtained was almost the same as 1.384.[36] Thus it is reasonable to assume that the difference in RI between the control group and the activated group in the current study is negligible. Conversely, high resolution DIC, confocal fluorescence, and living cell AFM images demonstrate that the complexity of cell structure and the roughness of cell surface are notably increased, and cells undergo cytoskeleton reorganization, after LPS/IFN-γ stimulation. Correlated to the changes

in cell structure and cell surface morphology, the backward scatter by the activated cells is increased revealed by the cell images taken with an OD = 2.0 NIR absorptive ND filter (Figure 4b). It is known that the backscatter was enhanced when light was scattered from random rough surfaces.[37] Since $<cos\theta>$ is the mean over the sphere of the cosine of the scattering angle, its value decreases when the ratio of forward-to-backward scatter decreases. If everything else remains the same in Equation [1], radiation pressure force F_{pr} is increased when backward scatter is enhanced as a result of increase in cell complexity and cell surface roughness.

In label-free flow cytometry analysis, the scattered light with larger angles are collected by a SSC detector positioned at 90° of the incident laser beam and cells with rougher surface and higher complexity display enhanced intensity of SSC-A. But unlike radiation pressure force analysis in which scattered light in every direction is accounted for, the collection angle of a SSC detector is limited and a significant portion of light scattered backward are not detected. Therefore cell velocity measurement in radiation pressure force analysis can achieve a much better population separation using far fewer cells (~ 600 cells) than label-free flow cytometry (> 50 K cells).

CONCLUSIONS

Using IC-21 macrophages as a model, we have shown that radiation pressure force analysis is capable of label free multi-parameter (cell velocity, size, and image) living cell analysis. The cell velocity which is inversely proportional to the magnitude of the radiation pressure force exhibits higher sensitivity than label-free flow cytometry in differentiating immune cell activation by LPS/IFN-γ, especially when changes in cell size and refractive index before and after the activation are insignificant. The higher sensitivity achieved in cell velocity based measurement arises from the prediction by Mie's theory that the amount of energy scatted and the angular distribution of the scattered light depend greatly on the form and composition of the particle and on the condition

of its surface.[18] Consequently it may be stated that the cell velocity based measurement by radiation pressure force analysis represents a "3D" scatter diagram of the cell. This work demonstrates that label-free microfluidic radiation pressure force analysis holds the potential to detect innate immune cell response to infection rapidly and sensitively.

CONFLICTS OF INTEREST

There are no conflicts of interest to declare.

ACKNOWLEDGEMENTS

The authors would like to acknowledge the Office of Naval Research and the Naval Research Laboratory for funding this research.

REFERENCES

[1] G. Gasteiger, A. D'Osualdo, D. A. Schubert, A. Weber, E. M. Bruscia and D. Hartl, *Innate Immun.*, 2017, **9**, 111–125.

[2] A. K. Abbas, A. H. Lichtman and S. Pillai, *Cellular and Molecular Immunology,* Elesvier Sanders, Philadelphi, PA, 2015, 76-78.

[3] M. Orecchioni, Y. Ghosheh, A. B. Pramod and K. Ley, *Front. Immunol.,* 2019, **10**, article 1084.

[4] S. Gordon, *Nat. Rev. Immunol.*, 2003, **3**, 23–35.

[5] C. D. Mills, K. Kincaid, J. M. Alt, M. J. Heilman and A. M. Hill, *J. Immunol.*, 2000, **164**, 6166-6173.

[6] G. Venter, F. T. J. J. Oerlemans, M. Wijers, M. Willemse, J. A. M. Fransen and B. Wieringa, *PLOS ONE*, 2014, **9**, e96786.

[7] N. Pavillona, A. J. Hobroa, S. Akirab and N. I. Smith, *PNAS*, 2018, **115**, E2676-E2685.

[8] H. M. Rostam, P. M. Reynolds, M. R. Alexander, N. Gadegaard and A. M. Ghaemmaghami, *Sci. Rep.*, 2017, **7***,* 3521.

[9] T. R. Carey, K. L. Cotner, B. Li and L. L. Sohn, *Nanomed. Nanobi*., 2019, **11**, e1529.

[10] A. Ashkin, *Phys.Rev. Lett.,* 1970, **24**, 156-159.

[11] A. Ashkin, J. M. Dziedzic and T. Yamanet, *Nature*, 1987, **330**, 769-771.

[12] J. Guck, S. Schinkinger, B. Lincoln, F. Wottawah, S. Ebert, M. Romeyke, D. Lenz, H. M. Erickson, R. Ananthakrishnan, D. Mitchell, J. Kȁs, S. Ulvick and C. Bilb, *Biophys. J*., 2005, **88**, 3689–3698.

[13] T, Kolb, S. Albert, M. Haug and G. Whyte, *J. Biophotonics*, 2015, **8**, 239–246.

[14] T. Imasaka, Y. Kawabata, T. Kaneta and Y. Ishidzu, *Anal. Chem.*, 1995, **67**, 1763-1765.

[15] T. Kaneta, J. Makihara and T. Imasaka, *Anal. Chem.*, 2001, **73**, 5791-5795.

[16] C. G. Hebert, N. DiNardo, Z. L. Evans, S. J. Hart and A.-B. Hachmann, *Vaccine*, 2018, **36**, 6061–6069.

[17] H. Kobayashi, C. Lei, Y. Wu, C.-J. Huang, A. Yasumoto, M. Jona, W. Li, Y. Wu, Y. Yalikun, Y. Jiang, B. Guo, C.-W. Sun, Y. Tanaka, M. Yamada, Y. Yatomi and K. Goda, *Lab Chip*, 2019, **19**, 2688–2698.

[18] H. C. Van de Hulst, *Light Scattering by Small Particles*, Wiley, New York, 1957.

[19] W. S. Walker and A. Demus, *J. Immunol*., 1975, **114**, 765-769.

[20] B. Tu, A. Wallin, P. Moldeus and I. A. Cotgreave, *Toxicology,* 1995, **104**, 159-164.

[21] M. D. Sawyer, T. van Raaij, J. Cross and B. E. Sumpio, *Arch. Surg*. 1998, **133**, 438-441.

[22] F. Y. Liew, 1994, **43**, 95-98.

[23] D. M. Mosser and X. Zhang, *Curr. Protoc. Immunol*., 2008, **83**, 14.2.1-14.2.8.

[24] K. A. Jablonski, S. A. Amici, L. M. Webb, J. de D. Ruiz-Rosado, P. G. Popovich, S. Partida-Sanchez and M. Guerau-de-Arellano, *PLOS ONE*, 2015, **10**, 0145342.

[25] R. Tang, G. Zhang and S.-Y. Chen, *J. Biol. Chem.,* 2014, **289**, 22715–22722.

[26] S. D. Hansen and R. D. Mullins, *J. Cell Biol.*, 2010, **191**, 571–584.

[27] A. Tzur1, J. K. Moore, P. Jorgensen, H. M. Shapiro and M. W. Kirschner, *PLOS ONE*, 2011, **6**, e16053.

[28] F. Hassan, S. Islam, N. Koide, M. M. Mu, H. Ito, I. Mori, T. Yoshida and T. Yokochi, Microbiol. Immunol., 2004, **48**, 807–815.

[29] F. Amano and Y. Akamatsu, *Infect. Immun.*, 1991, **59**, 2166–2174.

[30] K. Yoshida, M. Ono and H. Sawada, *J. Endotoxin Res.*, 1999, **5**, 127-137.

[31] J. Pi, T. Li, J. Liu, X. Su, R. Wang, F. Yang, H. Bai, H. Jin and J. Cai, *Micron*, 2014, **65**, 1–9.

[32] M. Kerker, *The scattering of light and other electromagnetic radiation: physical chemistry: a series of monographs*; Academic press: New York, London, 1969.

[33] *Fundamental Optics, The CVI Melles Griot Technical Guide*; CVI Melles Griot, 2009, 2.

[34] Q. Lu, D. E. Barlow, D. Haridas, B. C. Giordano, H. D. Ladouceur, J. D. Gaston, G. E. Collins and A. V. Terray, *ACS Omega*, 2019, **4**, 12938−12947.

[35] V. A. Markel, *J. Opt. Soc. Am. A,* 2016, **33**, 1244−1256.

[36] C. G. Hebert, S. Hart, T. A. Leski, A. Terray and Q. Lu, *Anal. Chem.*, 2017, **89**, 10296–10302.

[37] E. R. Mendez and K.A. O'Donnell, *Opt. Commun.,* 1987, **61**, 91-95.

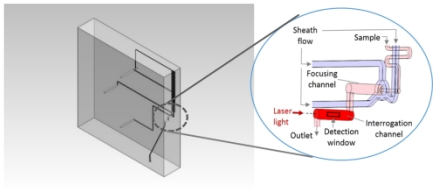

Figure 1 Schematic of the microfluidic flow cell.

338x190mm (230 x 230 DPI)

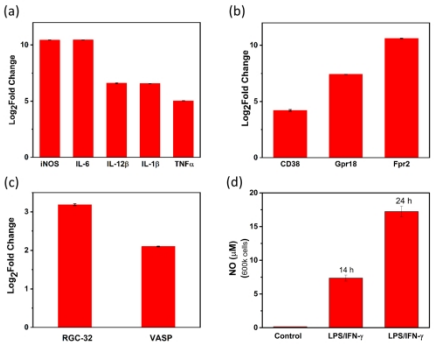

Figure 2 Gene expression changes and nitric oxide production in IC-21 cells activated with LPS/IFN-γ. (a) Log_2Fold change in gene expression of iNOS, IL-6, IL-12β , IL-1β, and TNFα, (b) Log_2Fold change in gene expression of M1-distinct genes CD38, Gpr18, and Fpr2, (c) Log_2Fold change in gene expression of RGC-32 and VASP, after 24 h LPS/IFN-γ stimulation. (d) Nitric oxide production (600K cells) after 14 and 24 h stimulation with LPS/IFN-γ.

338x190mm (230 x 230 DPI)

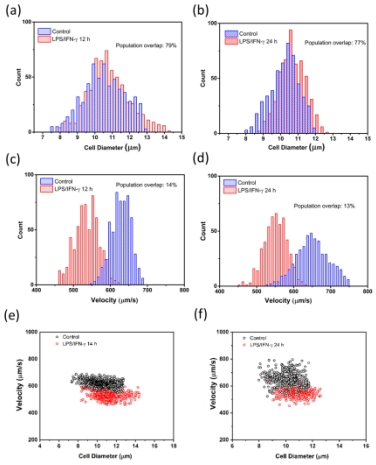

Figure 3. Radiation pressure force analysis of IC-21 cells before and after LPS/IFN-γ stimulation. (a) and (b) Comparison of histograms of the cell diameters between the control group and the activated group after 14 or 24 h stimulation. (c) and (d) Comparison of histograms of the cell velocities between the control group and the activated group after 14 or 24 h stimulation.

338x190mm (230 x 230 DPI)

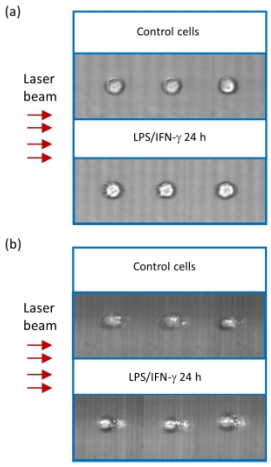

Figure 4. (a) Cell images captured during radiation pressure force analysis by the CCD camera from the control and the activated group (24 h) using an OD = 3.0 NIR absorptive ND filter. (b) Cell images from the control and the activated group (24 h) with observable scattered laser light captured using an OD= 2.0 NIR absorptive ND filter.

338x190mm (230 x 230 DPI)

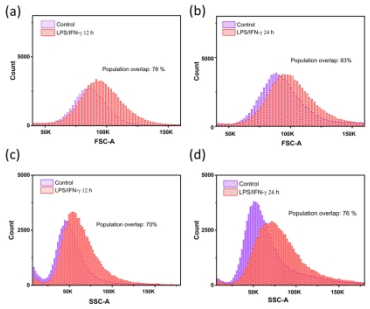

Figure 5. Flow cytometry analyses of IC-21 cells before and after LPS/IFN-γ activation. (a) and (b) Comparison of histograms of FSC-A between the control and the activated group after 14 or 24 h stimulation. (c) and (d) Comparison of histograms of SSC-A between the control and the activated group after 14 or 24 h stimulation.

338x190mm (230 x 230 DPI)

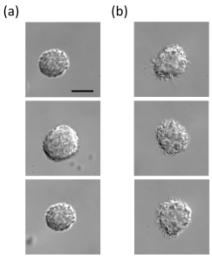

Figure 6 DIC images of fixed suspension cells from (a) the control group and (b) the activated group (24 h), scale bar: 10 μm .

338x190mm (230 x 230 DPI)

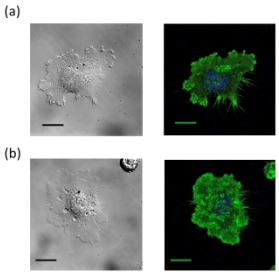

Figure 7 DIC and confocal fluorescence microscopy images of fixed adherent cells from (a) the control group and (b) the activated group (24 h). Green: actin filament stain, blue: DAPI nuclear stain. Scale bar: 10 μm.

338x190mm (230 x 230 DPI)

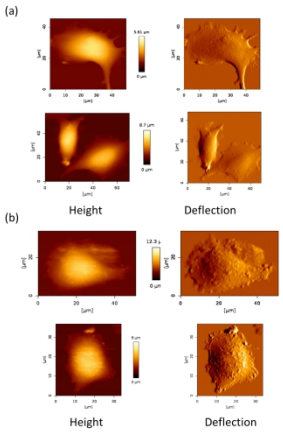

Figure 8 AFM images of live IC-21 cells from (a) the control group and (b) the activated group (24 h).

338x190mm (230 x 230 DPI)